Energy band structure of strained $Si_{1-x}C_x$ alloys on Si (001) substrate

S. T. Chang
Department of Electrical Engineering and Graduate Institute of Electronic Engineering, National Taiwan University, Taipei, Taiwan, Republic of China

C. Y. Lin[a)]
Department of Physics, National Chung Hsing University, Taichung, Taiwan, Republic of China

C. W. Liu
Department of Electrical Engineering and Graduate Institute of Electronic Engineering, National Taiwan University, Taipei, Taiwan, Republic of China

(Received 26 February 2002; accepted for publication 1 July 2002)

We report the energy band structures of strained $Si_{1-x}C_x$ alloys on Si (001) substrates. All calculations are based on a 20×20 Hamiltonian matrix constructed from the linear combination of atomic orbital approximation with spin–orbit interaction, strain effect, and lattice disorder effect taken into account. The lattice disorder parameter is obtained from fittings with the experimental band gap of strained $Si_{1-x}C_x$ alloy with small carbon concentration and reflects the initial reduction of band gap of relaxed $Si_{1-x}C_x$ alloy, while simple virtual crystal approximation does not. The effect of strain on band structure is incorporated in terms of the interatomic interaction parameters, which are functions of bond length and bond angle. The strained $Si_{1-x}C_x$ alloy becomes metallic when $x=28\%$. All the directional effective masses are affected by the strain. Overall agreements are found between our theoretical calculations and recent experimental results. © *2002 American Institute of Physics.* [DOI: 10.1063/1.1502203]

I. INTRODUCTION

The potential applications of high speed electronics and optoelectronics using SiGe materials have stimulated great interests in investigating column IV binary and ternary alloys.[1,2] However, the device performance is limited by the small critical thickness of these strained SiGe layers.[3] It has been shown that the incorporation of carbon can reduce the strain in these layers; high-quality SiGeC material with defect-free photoluminescence can be epitaxially grown[4] and the Si/SiGeC/Si heterojunction bipolar transistors have been successfully fabricated.[5] The out-diffusion of boron can be suppressed by the carbon incorporation.[6] Recently, high-quality pseudomorphic $Si_{1-x}C_x$ and $Si_{1-x-y}Ge_yC_x$ layers with the carbon concentration up to 7% are prepared by solid-source molecular beam epitaxy.[7] The substitutional C atoms in $Si_{1-x}C_x$ and related alloys also offer an additional parameter to tailor the energy band structure. The $Si/Si_{1-x}C_x/Si$ *pnp* heterojunction bipolar transistor was demonstrated by Singh.[8] The lattice constant of $Si_{1-x}C_x$ alloy is smaller than that of Si, so the strain condition of strained $Si_{1-x}C_x$ on Si is similar to that of the high mobility strained Si on relaxed SiGe.[9,10] Thus the $Si_{1-x}C_x$ channel embedded in Si has been proposed as an alternative to a strained Si channel. Since a graded buffer is not necessary for the fabrication of a strained $Si_{1-x}C_x$ layer, high crystalline perfection of a $Si_{1-x}C_x$ channel is obtained.[9,10] For theoretical work, most studies focused on band gap issues of SiGeC alloys. Soref, using the interpolation technique, gave a monotonic variation of band gaps of SiGeC alloys.[11] Demkove and Sankey performed an *ab initio* tight-binding (TB) calculation on electronic structure and predicted a reduction of fundamental band gap in unstrained $Si_{1-x}C_x$ caused by a small amount of C in the Si lattice.[12] Later, Xie *et al.* using linear muffin tin orbital (LMTO) methods predicted similar results.[13] The previous calculations employed a supercell approach in which Si and C atoms with appropriate proportions were located on diamond lattice sites to simulate the random alloy. The alloy composition was thus limited to discrete points in composition parameter space. We perform the theoretical study on the band structures of both strained and relaxed $Si_{1-x}C_x$ alloys with continuous variation of carbon concentration that is useful for device design and simulation. Our calculations are based on the framework of linear combination of atomic orbits (LCAO)[14] with spin–orbit interaction,[15,16] strain, virtual crystal approximation (VCA),[17] and lattice disorder effect. The tight-binding atomic basis set consists of one s orbital, three p orbitals, and one excited s^* orbital per atom. We propose a lattice disorder parameter ΔV_{S*P} to reproduce the observed initial reduction of band gap of strained $Si_{1-x}C_x$, while previous LCAO calculactions[18] showed no such effect.

In Sec. II we discuss the theoretical considerations of our work, including the lattice disorder parameter and strain effect. Then in Sec. III we summarize and discuss our results. A summary is given in Sec. IV.

II. THEORY

A. Modified LCAO calculation of $Si_{1-x}C_x$ alloy

A set of semiempirical linear combination of atomic orbits is used to calculate the energy band structure of the relaxed $Si_{1-x}C_x$ bulk alloy.[16] The second nearest neighbor

[a)]Author to whom correspondence should be addressed; electronic mail: cylin@nchu.edu.tw

 © 2002 American Institute of Physics

Downloaded 12 Feb 2009 to 140.112.113.225. Redistribution subject to AIP license or copyright; see http://jap.aip.org/jap/copyright.jsp

TABLE I. Energy band structure parameters for the sp^3s^* tight-binding band calculation.

	Si	C	$Si_{1-x}C_x$
$Es(000)$	−4.813 41	−3.810 00	
$Ep(000)$	1.775 63	3.220 00	Linear interpolation
$Es^*(000)$	5.613 42	16.000 00	
$4\times Vss\sigma(0.5\,0.5\,0.5)$	−8.332 55	−17.220 00	
$4\times Vpp\sigma(0.5\,0.5\,0.5)$	12.281 01	26.140 00	
$4\times Vpp\pi(0.5\,0.5\,0.5)$	−3.591 80	−8.420 00	Eq. (1)
$4\times Vsp\sigma(0.5\,0.5\,0.5)$	10.152 20	17.410 01	
$4\times Vs^*p\sigma(0.5\,0.5\,0.5)$	8.450 01	3.706 01	
$4\times Vss(110)$	0.015 91	0.000 00	
$4\times Vsx(110)$	0.080 02	0.400 10	
$4\times Vsx(011)$	−1.316 99	0.000 00	
$4\times Vs^*x(110)$	−0.005 79	−0.000 41	
$4\times Vs^*x(011)$	−0.501 03	−0.040 13	
$4\times Vxx(110)$	0.121 91	3.920 02	Linear interpolation
$4\times Vxx(011)$	−0.106 61	−2.024 01	
$4\times Vxy(110)$	0.550 67	−0.149 61	
$4\times Vxy(011)$	2.277 84	0.000 41	
$C_{12}(10^{12}\ \mathrm{cm^2/dyne})$	0.64	1.25	
$C_{11}(10^{12}\ \mathrm{cm^2/dyne})$	1.65	10.76	
a [Å]	5.431	3.566	
Affinity (eV)	4.05	2.30	

interaction is considered and the sp^3s^* orbitals of each atom are taken as the basis functions. Spin–orbit splitting is taken into account based on the method given in Refs. 15 and 16. Therefore the final matrix is of size 20×20. Slater–Koster (SK)[19] integral parameters are adopted and parameters used for bulk Si and C are given in Table I. To calculate the energy band structure of the $Si_{1-x}C_x$ alloy, the VCA is assumed to obtain parameters of $Si_{1-x}C_x$ alloys. The nearest neighbor distance d, the on site matrix elements, and the second-neighbor parameters are linearly interpolated as functions of carbon molar fraction x, while the first nearest neighbor parameters are interpolated in accordance with Harrison's d^{-2} rule:[17]

$$V_{\text{alloy}}=\left(\sum_{i=\text{Si,C}} d_i x_i\right)^{-2}\sum_{i=\text{Si,C}}(d_i)^2 x_i V_i, \tag{1}$$

where V_{alloy} and V_i are particular empirical SK parameters for the alloy and elemental end points, respectively, and d_i is the appropriate first nearest neighbor distance in crystalline Si and C. Finally, x_i is the atomic fraction of each elemental component. The interpolation method applied for relaxed $Si_{1-x}C_x$ alloys is also indicated in Table I. The leading factor in Eq. (1) represents the inversed square of the first nearest neighbor distance in the alloy; here we assume that Vegard's law is valid for these alloys, and obtain the nearest neighbor distances by linear interpolation. The assumption is thus made that the symmetry of the alloy remains perfectly tetrahedral. Note that this VCA does not include the local strain as reported in Ref. 18.

The band gap shrinkage is due to the local strain around the substitutional C atoms, which are randomly distributed in the $Si_{1-x}C_x$ alloys.[12,13] Since the bond length of a Si–C bond in random $Si_{1-x}C_x$ alloys for small C concentration is smaller than the one obtained from Vegard's law,[20] the TB parameter V_{s*p} in the relaxed $Si_{1-x}C_x$ alloy must be increased accordingly, as compared to that of the original virtual-crystal approximation. The modified TB parameter V_{s*p} is thus written empirically as

$$V_{s*p}(\text{modified})=V_{s*p}(\text{original})+\Delta V_{s*p}x(1-x), \tag{2}$$

where x is the carbon molar fraction. The reason we use the modified term in Eq. (2) is that the difference in lattice constant between results obtained from Vegard's rule and Kelires' results[20] has a maximum value at $x=0.5$, and minima at both $x=0$ and 1. The term $\Delta V_{s*p}x(1-x)$ is defined as the "lattice disorder parameter."

The valence band edge of Si is taken as the energy level reference point. Referring to the Si valence band, the valence band offset between Si and C, $\Delta E_V(\text{C})=\Gamma_{25}^v(\text{C})-\Gamma_{25}^v(\text{Si})$, is added to C orbital energies. Similarly, the valence band offset between Si and $Si_{1-x}C_x$, $\Delta E_V(Si_{1-x}C_x)$ is added to $Si_{1-x}C_x$ orbital energies. Since the valence band edges of Si and C below vacuum are 5.17 and 7.8 eV, respectively, linear interpolation gives $\Delta E_V(Si_{1-x}C_x)=-2.63x$ eV.

B. Tight-binding parameters in strained $Si_{1-x}C_x$ alloy

Since the lattice constant of diamond does not match with that of Si, there are strains in the $Si_{1-x}C_x$ alloy layer grown along the z direction on Si (001) substrates. For simplicity, in this paper we restrict ourselves to the special case of a biaxial strain, namely,

$$\begin{aligned}&\varepsilon_{xx}=\varepsilon_{yy}\neq\varepsilon_{zz},\\&\varepsilon_{xy}=\varepsilon_{yz}=\varepsilon_{zx}=0.\end{aligned} \tag{3}$$

For the case of strained SiC alloy on Si (001) substrates, we obtain

$$\begin{aligned}&\varepsilon_{xx}=\varepsilon_{yy}=(a_{\text{sub}}-a)/a,\\&\varepsilon_{zz}=-2(C_{12}/C_{11})\varepsilon_{yy},\end{aligned} \tag{4}$$

where a_{sub} and a are the lattice constants of the Si substrates and $Si_{1-x}C_x$ alloys, respectively, and C_{11} and C_{12} are the stiffness constants as shown in Table I. Assuming uniform deformation of the diamond-like unit cell, vectors connecting nearest neighbor atoms in the strained $Si_{1-x}C_x$ alloy layer have the form

$$\vec{d}=\frac{a}{4}\{\pm(1+\varepsilon_{xx})\hat{x}\pm(1+\varepsilon_{yy})\hat{y}\pm(1+\varepsilon_{zz})\hat{z}\}. \tag{5}$$

Here $\hat{x}$, $\hat{y}$, and $\hat{z}$ are unit vectors along the coordinate axes, which are the unit cell edges. The length of the vector $\vec{d}$ is

$$d=\frac{a}{4}\sqrt{3+4\left[1-\left(\frac{C_{12}}{C_{11}}\right)\right]\varepsilon_{xx}+2\left[1+\left(\frac{C_{12}}{C_{11}}\right)^2\right]\varepsilon_{xx}^2}. \tag{6}$$

Direction cosines between the vector $\vec{d}$ and the x, y, and z axes are thus given by

$$l_x=l_y=(1+\varepsilon_{xx})\Big/\sqrt{3+4\left[1-\left(\frac{C_{12}}{C_{11}}\right)\right]\varepsilon_{xx}+2\left[1+\left(\frac{C_{12}}{C_{11}}\right)^2\right]\varepsilon_{xx}^2} \tag{7}$$

and

Downloaded 12 Feb 2009 to 140.112.113.225. Redistribution subject to AIP license or copyright; see http://jap.aip.org/jap/copyright.jsp

$$l_z=[1-2(C_{12}/C_{11})\varepsilon_{xx}] \Big/ \sqrt{3+4\left[1-\left(\frac{C_{12}}{C_{11}}\right)\right]\varepsilon_{xx}+2\left[1+\left(\frac{C_{12}}{C_{11}}\right)^2\right]\varepsilon_{xx}^2}. \quad (8)$$

For the off-diagonal TB parameters between atoms, Eqs. (7) and (8) are used to modify the nearest neighbor TB parameters as in Ref. 19. The dependence of the smaller second-nearest neighbor TB parameters on bond angles is not so important and therefore is neglected here. The change of the bond length dependence of the nearest and second-nearest neighbor modifies the off-diagonal TB parameters between different atoms V_{ij} according to the empirical scaling rule[21] [Eq. (9)], which are applicable to all matrix elements, except V_{s*px}, V_{s*py}, and V_{s*pz}. The elements V_{s*px}, V_{s*py}, and V_{s*pz} will be described later.

$$V_{ij}=V_{ij}^0\left(\frac{d_0}{d}\right)^{-n(ij)}, \quad (9)$$

where V_{ij}^0 and V_{ij} are the unstrained and strained TB parameters, respectively, for the interactions between state i and state j; d_0 and d are the unstrained and strained bond lengths, respectively, and $n(ij)$ is the scale index. In order to incorporate the influence of the strain into the electronic band structure correctly, the scale index $n(ij)$ is determined from fittings with the experimental values of the hydrostatic deformation potential for the first nearest neighbor. The dependence of the second-nearest neighbor TB parameters on bond lengths is taken as $n(ij)=2$, similar to Harrison's d^{-2} rule. The correct values of hydrostatic deformation potentials can be obtained by adjusting the scale index $n(ij)$.[21,22] Equation (10) is used to combine both bond length and bond angle effects.

$$\begin{aligned}
&V_{ii}=l_i^2V_{pp\sigma}+(1-l_i^2)V_{pp\pi},\\
&V_{ij}=l_il_jV_{pp\sigma}-l_il_jV_{pp\pi},\\
&V_{spi}=l_iV_{sp\sigma}, \qquad (10)\\
&V_{ss}=V_{ss\sigma},\\
&i\neq j, \quad i,j=x,\ y,\ z.
\end{aligned}$$

Incorrect shear deformation potentials may result in a wrong order of energies for the splitting levels among the six conduction band valleys at Δ points under the uniaxial strain.[23] In order to account for the variations of the energy band structures by the uniaxial strains correctly, a new scale index F is introduced according to the method proposed by Munoz and Armells.[23] In this method the TB parameters between s^* and $p(p_x,p_y,p_z)$ states are given as functions of strain components $\varepsilon_{xx}=\varepsilon_{yy}$, and ε_{zz} in the following way:

$$V_{s^*p_x}=V_{s^*p_y}=\left(\frac{d}{d_0}\right)^{n(s^*p)+1} V_{s^*p_x}^0[(1+\varepsilon_{xx})-F(\varepsilon_{zz}-\varepsilon_{xx})], \quad (11)$$

TABLE II. The scaling indices $n(ij)$ for our calculation.

Material\n(ij)	$n(ss)$	$n(sp)$	$n(s^*p)$	$n(xx)$	$n(xy)$
Si	3.2	1.8	2.5	2.7	3.3
C	3.4	1.4	2.6	2.0	3.3

$$V_{s^*p_z}=\left(\frac{d}{d_0}\right)^{n(s^*p)+1} V_{s^*p_z}^0[(1+\varepsilon_{zz})+2F(\varepsilon_{zz}-\varepsilon_{xx})]. \quad (12)$$

The new scale index, F, is determined from fittings with the experimental values of shear deformation potential. The value of F used in our calculation is -0.9. The diagonal matrix element E_p is calculated from Ref. 22 as

$$E_p^{(x,y)}=E_p+b_p(\varepsilon_{xx}-\varepsilon_{zz}), \quad E_p^{(z)}=E_p-b_p(\varepsilon_{xx}-\varepsilon_{zz}). \quad (13)$$

The E_s and E_{s*} terms remain the same under uniaxial strain. The uniaxial deformation potential b_p of p-orbital energies is chosen to be 1.735 eV that fits the experimental uniaxial splitting of hole energies of silicon. The larger value of 6.441 eV is used for carbon in our calculation.

C. Values of scaling indices $n(ij)$ and deformation potentials

The scaling index $n(ij)$ is determined from fittings with the hydrostatic deformation potential constants. Under the strains, the energy levels of the conduction band on the Δ axis and valence band edge at the Γ point are given in Refs. 22 and 24. The fitted indices $n(ij)$ of Si and C are listed in Table II. The indices $n(ij)$ of $Si_{1-x}C_x$ alloy are obtained by the linear interpolation between Si and C values. The values of the deformation potential used in our work are listed in Table III as well as the experimental data. Deformation potentials Ξ_U^{Δ} are obtained from the splitting values between Δ_{XY} valleys (the valleys perpendicular to growth direction) and Δ_Z valleys (the valleys along the growth direction) under the uniaxial strain, and b is obtained from the splitting values of the valence band levels under the uniaxial strain.

III. RESULTS AND DISCUSSION

In order to account for the band gap shrinkage of relaxed $Si_{1-x}C_x$ at low carbon content, the lattice disorder parameter

TABLE III. The deformation potentials of Si and C. The column labeled "Exp." gives the experimental values, and the column labeled "TB" gives the values obtained in this work.

	Si		C	
	TB	Exp.	TB	Exp.
b	−2.33	−2.33[a]	−1.65	−1.65[d]
Ξ_u^{Δ}	9.26	9.2[b]	34.9	
$\Xi_d^{\Delta}+\Xi_u^{\Delta}/3-a_v$	1.5	1.5[c]	−2.3	−2.3[e]

[a]Reference 25.
[b]Reference 26.
[c]Reference 27.
[d]Reference 28.
[e]Reference 29.

Downloaded 12 Feb 2009 to 140.112.113.225. Redistribution subject to AIP license or copyright; see http://jap.aip.org/jap/copyright.jsp

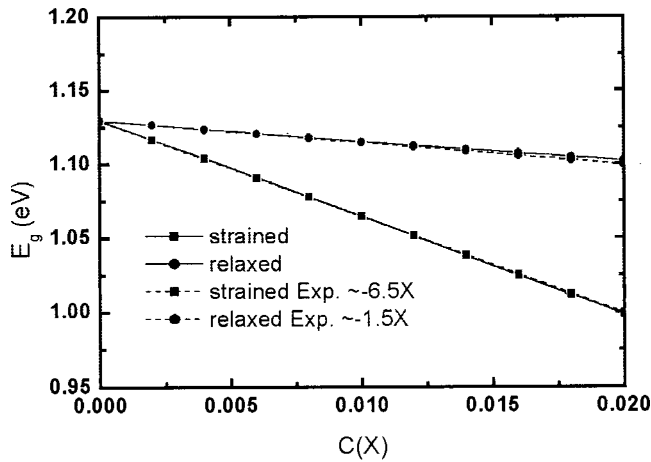

FIG. 1. The band gap for relaxed and strained $Si_{1-x}C_x$ alloy as a function of the alloy composition $x(x<2\%)$, where solid lines and dashed lines are results from our work and the PL measurement,[30,31] respectively.

ΔV_{s*p} is used. The value of $\Delta V_{s*p}=3.4\,\mathrm{eV}$ is extracted from fittings with the experimental band gap of strained $Si_{1-x}C_x$ alloys.[30,31] The band gap for relaxed and strained $Si_{1-x}C_x$ alloy as a function of the alloy composition x is shown in Fig. 1, where solid lines and dashed lines denote results of our work and the PL measurement, respectively. The experimental data are given with $x<2\%$. From Fig. 1, our work is in good agreement with those extracted from the PL measurement. The energy gaps for all values of the alloy composition x of the relaxed $Si_{1-x}C_x$ alloy are given in Fig. 2, together with those from Xie's model[13] and Demkov and Sankey's model.[12] Our calculation shows that as x varies from 0 to 0.02 in $Si_{1-x}C_x$, the band gap decrease with x, with values $\Delta E_g \sim -1.5x$, and reaches the lowest points at $x=0.12$. Further increase of carbon concentration results in a monotonically increasing of the band gap. The band gap shrinkage of $Si_{0.984}C_{0.016}$ is about 23 meV from our model, considerably smaller than the values of 170 and 50 meV calculated from Demkov and Sankey's model[12] and Xie's model,[13] respectively (the inset of Fig. 2). The band gap

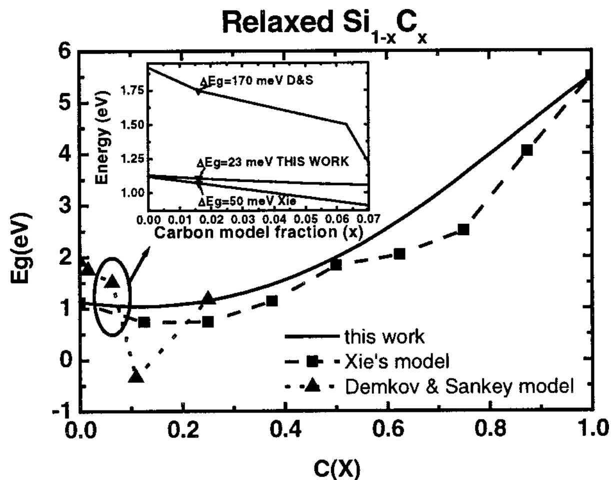

FIG. 2. The energy gaps of relaxed $Si_{1-x}C_x$ alloy as a function of the alloy composition x. The inset is the close-up view for small carbon concentration.

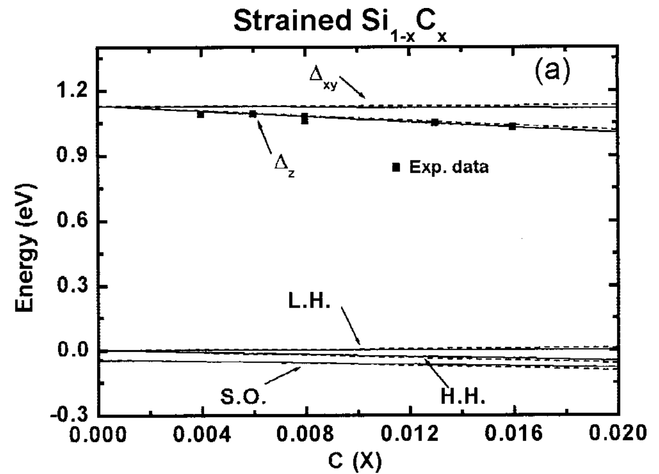

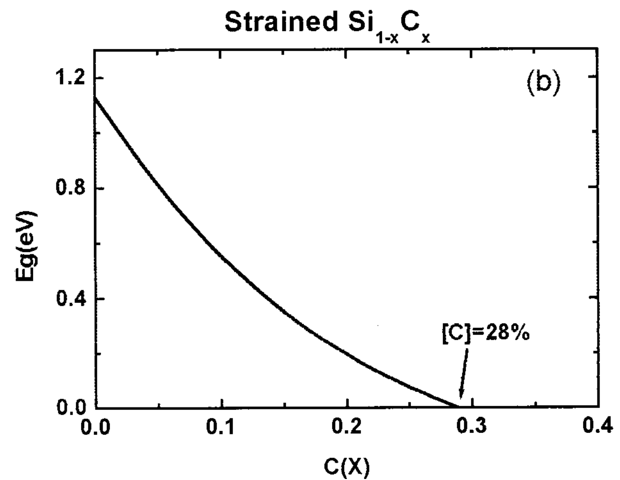

FIG. 3. (a) Energetical position of conduction (Δ_{XY} and Δ_Z) and valence band edges (heavy-, light-, and spilt-off-hole) of a strained $Si_{1-x}C_x$ layer on Si (001) substrates calculated from our model (solid line) and deformation potential theory (dashed lines). For comparison, the experimental data from Refs. 9, 10, and 11 are also shown. (b) Energy gap of strained $Si_{1-x}C_x$ alloy as a function of the alloy composition x.

shrinking is due to the local strain around the substitutional C atoms, which are randomly distributed in the $Si_{1-x}C_x$ alloy. The reduction of the band gap ceases to appear due to the fact that local disorder effects could only be significant in a low concentration of carbon in a $Si_{1-x}C_x$ alloy. We successfully use modified TB parameter ΔV_{s*p} to include the effect of this local disorder in $Si_{1-x}C_x$ alloys.

In order to check the validity of our model of strain effects, we compare our results for strain-induced shifts of band edges with our calculation based on the simple phenomenological deformation potential method[22,24] using the relaxed band gap in Fig. 2. We calculate the energies of the valence band edges of heavy hole (HH), light hole (LH), and split-off hole (SO), and conduction band minimum (Δ_{XY} and Δ_Z) as a function of x for strained $Si_{1-x}C_x$ grown coherently on (001) Si substrates. The results of our model and results of the deformational potential method are shown in Fig. 3(a) together with the experimental data.[9,10] The discrepancies of the shift of valence and conduction band edges between the two approaches are generally small. We also predict that the strained $Si_{1-x}C_x$ alloy becomes metallic when $x=0.28$ [Fig.

Downloaded 12 Feb 2009 to 140.112.113.225. Redistribution subject to AIP license or copyright; see http://jap.aip.org/jap/copyright.jsp

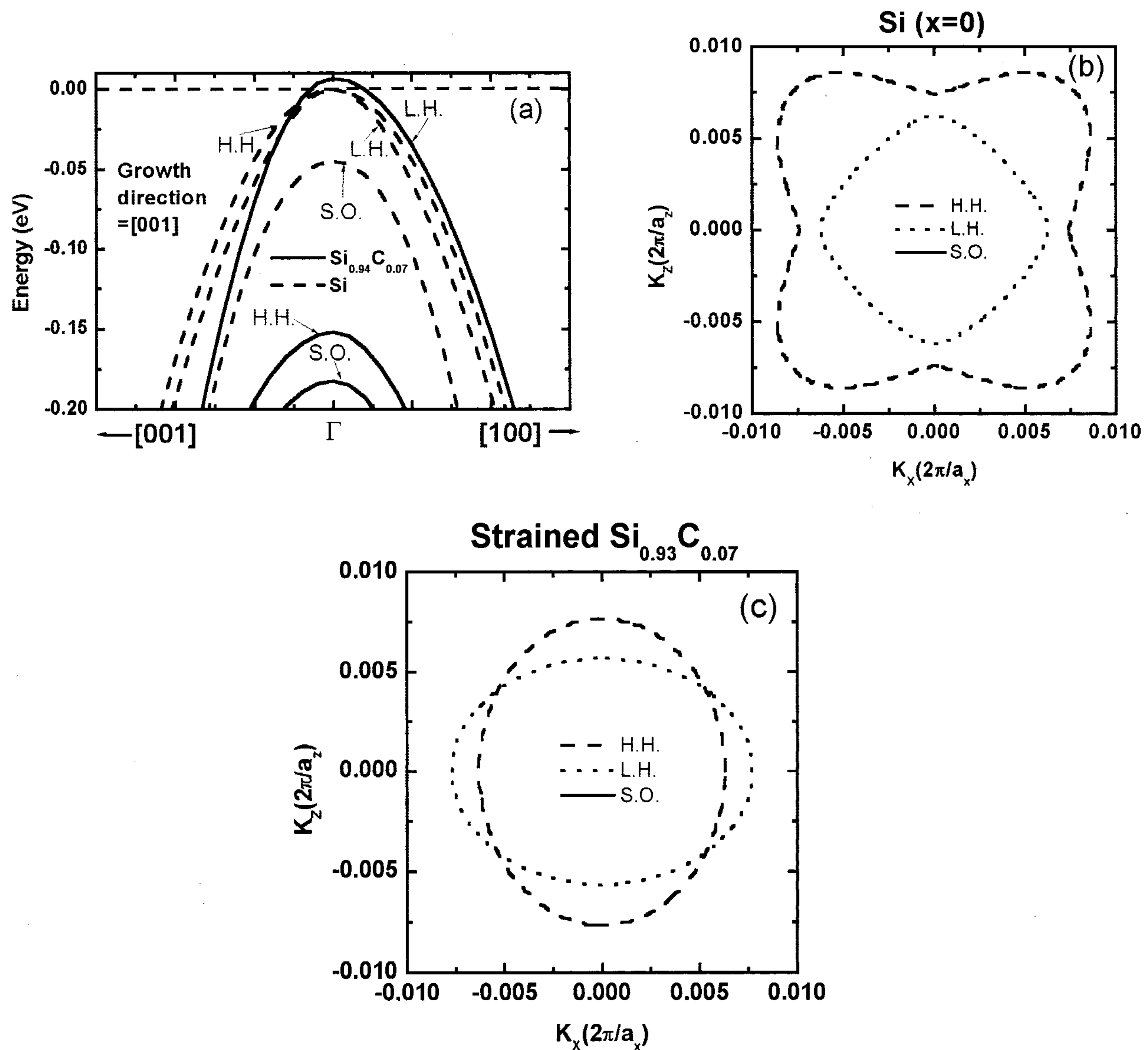

FIG. 4. (a) Energy spectra for the heavy hole (HH), light hole (LH), and split-off hole (SO) bands for Si (dashed) and strained $Si_{0.93}C_{0.07}$ (solid). (b) Constant-energy contours for Si. (c) Constant-energy contour for strained $Si_{0.93}C_{0.07}$. The energy values are 1 meV below the edges of each corresponding bands as shown in (a).

3(b)]. Selected results of valence band energy spectra for $Si_{0.93}C_{0.07}$ as well as pure Si are illustrated in Fig. 4(a), where the corresponding spectra of pure Si are consistent with known results. As expected, the biaxial strain introduces significant asymmetry. The heavy hole and light hole bands become nondegenerate at the Γ point. The light hole band moves upward and the heavy hole band moves downward by values consistent with Eberl's results.[30,31] The parabolicity of the split-off band is no longer retained due to this biaxial strain. The large energy splitting (~150 meV) between the heavy hole band and the light hole band edges indicates a larger hole population in the light hole band. Constant-energy contours for the three bands of Si and strained $Si_{0.93}C_{0.07}$ are shown in Figs. 4(b) and 4(c), respectively. The difference of constant-energy contours of energy 1 meV below the edge of the corresponding bands reflects the relative change in carrier effective mass from that of Si to strained $Si_{0.93}C_{0.07}$ alloys. Comparing Figs. 4(b) and 4(c), it can be seen that under the biaxial strains, the highly warped heavy hole contour changes and becomes split-off-hole-like.

The dispersion curves of the lowest conduction band of $Si_{0.93}C_{0.07}$ alloy under (001) tensile strain are shown in Fig. 5 as well as that of Si. The energy minimum occurs at the Δ_Z valley, as is expected for strained $Si_{0.93}C_{0.07}$. The Δ_{XY} valley remains at almost the same position as in the bulk Si. Thus the tensile strain causes an energy splitting between the Δ_Z valleys and Δ_{XY} valleys, and leads to the band gap reduction of strained $Si_{1-x}C_x$ alloys. These results agree with Hoyt's experiment and calculation.[9,10]

Next, we discuss the calculated carrier effective mass of strained and relaxed $Si_{1-x}C_x$ alloys. The effective mass here refers to the diagonal elements of an effective mass tensor, which simply reflects the "inverse of curvature" of band structure at the band-edge. The calculated hole effective mass of strained and relaxed $Si_{1-x}C_x$ alloys along the (001) growth direction (hereafter referred to as the longitudinal

Downloaded 12 Feb 2009 to 140.112.113.225. Redistribution subject to AIP license or copyright; see http://jap.aip.org/jap/copyright.jsp

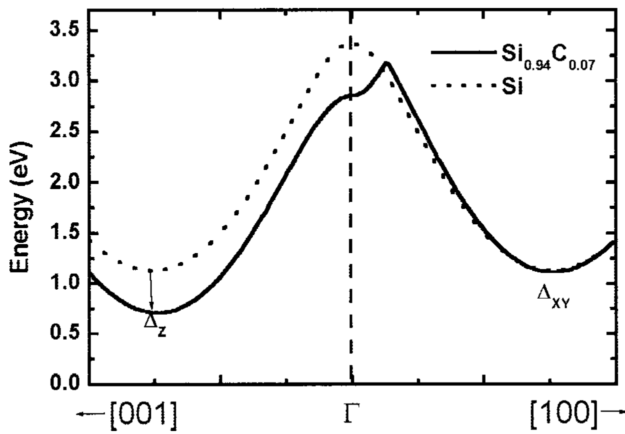

FIG. 5. Energy spectra for the lowest conduction band for Si (dashed line) and strained $Si_{0.93}C_{0.07}$ (solid line).

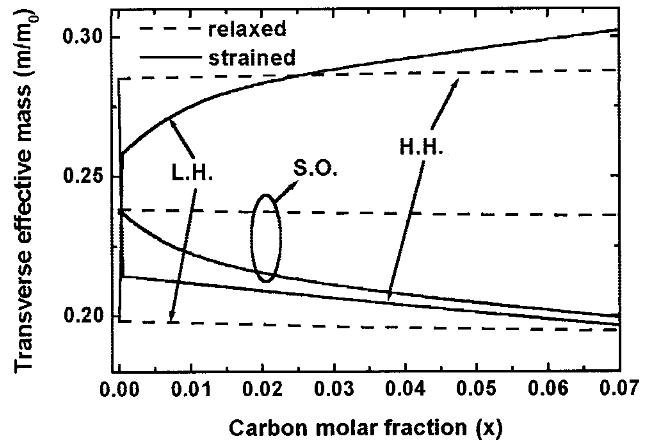

FIG. 7. Transverse hole effective masses at Γ point of $Si_{1-x}C_x$ alloy grown on (001) Si substrates. The solid lines are hole effective masses with strain and dashed lines are those without strain.

direction[32]) are shown in Fig. 6. With strain, the longitudinal light hole mass has the smallest change among these three hole bands since the light hole band in the growth direction does not strongly couple with the heavy hole or the spilt-off hole by the strain coupling terms. The strain, however, causes the heavy hole band interacting with the split-off band in the growth direction. In strained $Si_{1-x}C_x$, the light hole effective mass decreases with increasing x, while heavy hole and split-off hole effective mass increase with increasing x. The biaxial tensile strain results in an increase of the heavy hole effective mass and that of split-off holes, but the light hole effective mass decreases, as compare to the relaxed $Si_{1-x}C_x$. The transverse hole effective masses at the Γ point (perpendicular to the growth direction) for the strained $Si_{1-x}C_x$ alloy grown on (001) Si substrates are shown in Fig. 7. In strained $Si_{1-x}C_x$, the heavy hole effective mass decreases with increasing x with a significant drop at small carbon concentration. The split-off hole effective mass of strained $Si_{1-x}C_x$ decreases with increasing x smoothly, while light hole effective mass increases with increasing x with a sudden jump at the very low carbon concentration. Here, the definition of heavy and light hole needs to be clarified. At the Γ point, the heavy hole band is still primarily a $|3/2,3/2\rangle$ state for a small biaxial tensile strain. As the strain increases, the effect of strain-induced splitting energy begins to manifest, the heavy hole band (defined as $|3/2,3/2\rangle$ at the Γ point) switches to $|3/2,1/2\rangle$ at a small k. The value of k at which the exchange of the characters occurs depends on the strain, and the exchange can happen even at very small k values, which is also reported in Ref. 32. The strain effect on the transverse effective mass is opposite to the longitudinal directional case for heavy hole, light hole, and split-off hole bands. Namely, the biaxial tensile strain decreases the transverse effective mass of heavy hole and split-off bands, while increases that of the light hole band, as compared to relaxed $Si_{1-x}C_x$.

Finally, the electron effective masses at Δ_Z valleys of Fig. 5 are shown in Fig. 8. As compared to a hole, the strain changes the electron effective mass relatively small. The strain slightly decreases the transverse electron effective mass, and the transverse effective electron mass decreases

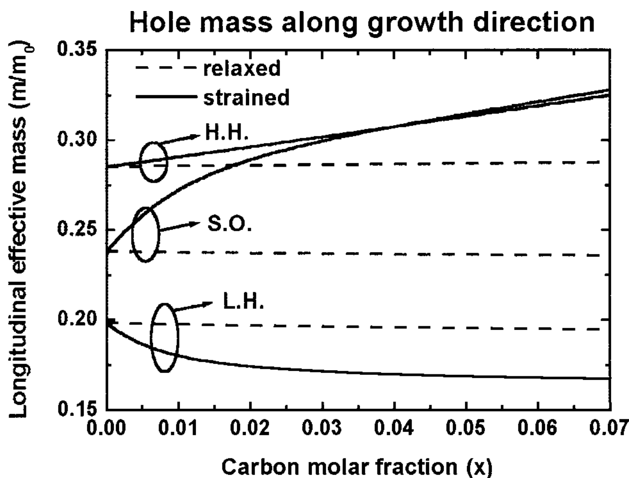

FIG. 6. Longitudinal hole effective masses at Γ point of a $Si_{1-x}C_x$ alloy grown on (001) Si substrates. The solid lines are hole effective masses with strain and dashed lines are those without strain.

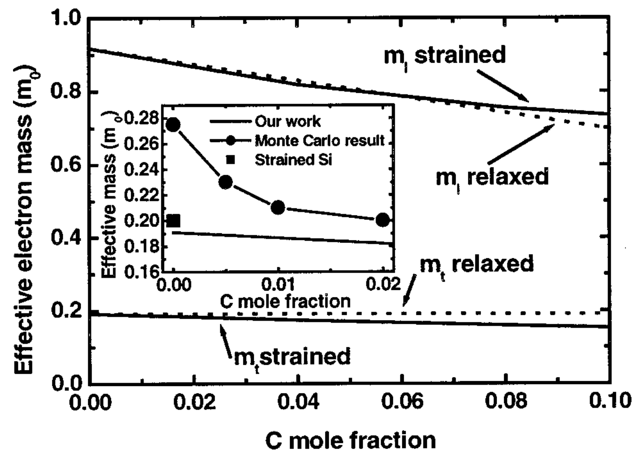

FIG. 8. Longitudinal electron effective mass m_l (along growth direction) and transverse electron effective mass m_t (perpendicular to growth direction) of $Si_{1-x}C_x$ alloy grown on (001) Si substrates at Δ_Z valleys. The solid lines are for alloys with strain and the dashed lines for alloys without strain. Comparison between our results and Monte Carlo simulation with a low electric field (1 kV/cm) is shown in the inset. The data of strained Si is obtained from Ref. 33.

Downloaded 12 Feb 2009 to 140.112.113.225. Redistribution subject to AIP license or copyright; see http://jap.aip.org/jap/copyright.jsp

with increasing x in strained $Si_{1-x}C_x$. Similar to our results, the experimental results[23] show that the transverse effective mass of strained Si does not change with strain significantly. As shown in the inset, our result of reduction of transverse effective electron mass qualitatively agrees with that of the Monte Carlo[34] simulation at the low electric field strength of 1 kV/cm.

IV. SUMMARY

In this work, we report calculation results of the relaxed and strained band structure of $Si_{1-x}C_x$ alloy considering the lattice disorder effect, strain effect, and spin–orbit interaction in the sp^3s^* tight-binding model. We predict that the strained $Si_{1-x}C_x$ alloy becomes metallic as $x=0.28$. We also calculate the carrier effective masses of strained and relaxed $Si_{1-x}C_x$ alloys. All the directional hole effective masses are effected by strain. As compared to hole, the electron effective masses are not sensitive to strain. Our theoretical calculations are in agreement with recent experimental data.

ACKNOWLEDGMENT

This work is supported by National Science Council, Taiwan, ROC, under Contract Nos. NSC90-2112-M-005-007, NSC90-2215-E002-034, and NSC90-2212-E002-224.

[1] S. J. Jeng, B. Jagannathan, J. S. Rieh, J. Johnson, K. T. Schonenberg, D. Greenberg, A. Stricker, H. Chen, M. Khater, D. Ahlgren, G. Freeman, K. Stein, and S. Subbanna, IEEE Electron Device Lett. **22**, 542 (2001).
[2] K. Washio, M. Kondo, E. Ohue, K. Oda, R. Hayami, M. Tanabe, H. Shimamoto, and T. Harada, IEEE Trans. Electron Devices **48**, 1989 (2001).
[3] J. L. Regolini, F. Gisbert, G. Dolino, and P. Boucaud, Mater. Lett. **18**, 57 (1993).
[4] C. W. Liu, A. St. Amour, Y. Lacroix, M. C. W. Thewalt, C. W. Magee, and D. Eaglesham, J. Appl. Phys. **80**, 3043 (1996).
[5] L. D. Lanzerotti, A. St. Amour, C. W. Liu, J. C. Sturm, J. K. Watanabe, and N. R. Theodore, IEEE Electron Device Lett. **17**, 334 (1996).
[6] H. Rucker, B. Heinemann, D. Bolze, D. Knoll, D. Kruger, R. Kurps, H. J. Osten, P. Schley, B. Tillack, and P. Zaumseil, Tech. Dig. - Int. Electron Devices Meet. **1999**, 345.
[7] K. Eberl, K. B. Vrunner, and W. Winter, Thin Solid Films **294**, 98 (1997).
[8] D. V. Singh, J. L. Hoyt, and J. F. Gibbons, Tech. Dig. - Int. Electron Devices Meet. **2000**, 749.
[9] J. L. Hoyt, T. O. Mitchell, K. Rim, D. Singh, and J. F. Gibbons, Mater. Res. Soc. Symp. Proc. **533**, 263 (1998).
[10] D. V. Singh, K. Rim, T. O. Mitchell, J. L. Hoyt, and J. F. Gibbons, J. Appl. Phys. **85**, 985 (1999).
[11] R. A. Soref, J. Appl. Phys. **70**, 2470 (1991).
[12] A. A. Demkov and O. E. Sankey, Phys. Rev. B **48**, 2207 (1993).
[13] J. Xie, K. Zcahng, and X. Xie, J. Appl. Phys. **77**, 3868 (1995).
[14] P. Vogl, H. P. Hjalmarson, and J. D. Dow, J. Phys. Chem. Solids **44**, 365 (1983).
[15] D. J. Chadi, Phys. Rev. B **16**, 790 (1997).
[16] C. Y. Lin and C. W. Liu, Appl. Phys. Lett. **70**, 1441 (1997).
[17] K. E. Newman and J. D. Dow, Phys. Rev. B **30**, 1929 (1984).
[18] B. A. Orner and J. Kolodzey, J. Appl. Phys. **81**, 6773 (1997).
[19] J. C. Slater and G. F. Koster, Phys. Rev. **94**, 1498 (1954).
[20] P. C. Kelires, Phys. Rev. B **55**, 8784 (1997).
[21] Z.-Z. Xu, Phys. Rev. B **47**, 3642 (1993).
[22] H. Rucker, R. Endeerlein, and F. Bechstedt, Phys. Status Solidi B **153**, 595 (1989).
[23] M. C. Munoz and G. Armelles, Phys. Rev. B **48**, 2839 (1993).
[24] G. L. Bir and G. E. Pikus, *Symmetry and Strain Induced Effects in Semiconductor* (Wiley, New York, 1974).
[25] M. M. Rieger and P. Vogl, Phys. Rev. B **48**, 14276 (1993).
[26] C. G. Van de Walle and R. M. Martin, Phys. Rev. B **34**, 5621 (1986).
[27] L. D. Laude, F. H. Pollak, and M. Cardona, Phys. Rev. B **3**, 2623 (1971).
[28] P. A. Crowther, P. J. Dean, and W. F. Sherman, Phys. Rev. **154**, 772 (1967).
[29] *Group IV Semiconducting Materials*, edited by M. Neuberger (Academic, New York, 1971), Vol. 5, p. 9.
[30] K. Brunner, K. Eberl, and W. Winter, Phys. Rev. Lett. **76**, 303 (1996).
[31] K. Eberl, K. Brunner, and W. Winter, Thin Solid Films **294**, 98 (1997).
[32] S. K. Chun and K. L. Wang, IEEE Trans. Electron Devices **39**, 2153 (1992).
[33] C. W. Liu and V. Venkataraman, Mater. Chem. Phys. **49**, 29 (1997).
[34] M. Ershov and V. Ryzhii, J. Appl. Phys. **76**, 1924 (1994).

Downloaded 12 Feb 2009 to 140.112.113.225. Redistribution subject to AIP license or copyright; see http://jap.aip.org/jap/copyright.jsp